Reduction Method of Current RMS Value, DC Current Ripple, and Radial Force Ripple for SRM based on Mathematical Model of Magnetization Characteristic

Takahiro Kumagai
Dept. of Science of Technology Innovation
Nagaoka University of Technology
Nagaoka, Japan
kumagai_t1125@stn.nagaokaut.ac.jp

Keisuke Kusaka
Dept. of Electrical, Electronics, and Information Engineering
Nagaoka University of Technology
Nagaoka, Japan
kusaka@vos.nagaokaut.ac.jp

Jun-ichi Itoh
Dept. of Science of Technology Innovation
Nagaoka University of Technology
Nagaoka, Japan
itoh@vos.nagaokaut.ac.jp

***Abstract*— This paper proposes a motor current RMS value, DC current ripple, and radial force ripple reduction method under zero torque ripple for switched reluctance motor (SRM). In the proposed method, the current waveform to achieve constant torque is derived based on a mathematical model of magnetization characteristic. In order to optimize multiple objective functions considering a trade-off relationship, the weight function is introduced. In particular, quantitative evaluation functions are derived from the mathematical model for avoidance of time-consuming numerical process. In the proposed method, it is possible to derive the desired current waveform for the motor current RMS value, the DC current ripple, and the radial force ripple by setting appropriate weights. The reduction of the motor current RMS value, DC current ripple, and radial force ripple by 18%, 45%, and 37%, respectively, are confirmed.**

Keywords—Switched reluctance motor, Instantaneous current control, Multi-objective optimization

I. INTRODUCTION

Switched Reluctance Motor (SRM) has potential for the application of hybrid electric vehicle (HEV) and electric vehicle (EV) thanks to its rare earth-element-free and low manufacturing cost, and suitability for high speed. In SRM, continuous rotation is achieved by excitation of each phase stator winding at an appropriate timing. However, a large torque ripple occurs during the switching phase interval due to insufficient torque. Therefore, the excitation of two-phase stator windings during the switching phase interval is applied to reduce the torque ripple [1]-[10]. In those methods, several current waveforms which generate the constant torque are obtained. The current waveform which generates the constant torque is referred as the constant-torque current waveform in Ref.[9]. Nevertheless, this method increases the current root-mean-square (RMS) value because the torque is generated during the interval of small torque per current value. In addition, DC current ripple occurs in the input of the inverter because the magnetic energy oscillation occurs between load and power supply even if the output torque is constant. Furthermore, the radial force ripple occurs in SRM due to the excitation during the alignment state where the radial force per current value is large. In order to solve the above problems, the constant-torque current waveform should be optimized in consideration of all above criteria.

In general, the desired constant-torque current waveform is selected from several waveforms derived by the variation of the parameters value, determining the shape of the current waveform [3], [4]. However, the optimization is time-consuming and needs to be conducted whenever the motor is changed. In Ref.[5]-[8] , the weight factors for the voltage limitation and the current reduction are derived. However, the DC current ripple and the radial force ripple are not considered in the optimization of the constant-torque current waveform. In addition, the computation requires time-consuming numerical process due to the large amounts of data of flux linkage and torque. Meanwhile, the optimization method for the motor current RMS value reduction under zero torque ripple has also been proposed [9]. However, the DC current ripple and the radial force ripple increase when the motor current RMS reduction method is applied. In other words, the design method considering all above criteria has not been considered.

This paper proposes a multi-objective optimization based on a mathematical model for the constant-torque current waveform considering the motor current RMS value, the DC current ripple, and the radial force ripple. In order to conduct the multi-objective optimization for the current waveform, the weight functions are introduced for each criteria. The originality of this paper is that the desired current waveform considering the motor current RMS value, the DC current ripple, and the radial force is achieved with setting appropriate weights. In particular, the relationship between the parameters value determining the shape of the current waveform and all above criteria is clarified. In addition, the optimization is conducted without any time-consuming numerical process by deriving quantitative evaluation functions of the motor current RMS value, the DC current ripple, and the radial force based on the mathematical model of the magnetization characteristic.

978-1-7281-3153-5/19/$31.00 ©2019 IEEE

II. Torque Ripple Reduction Method

A. Torque generation

Table I shows the motor parameters of the evaluated SRM. A three-phase 18S/12P type SRM is chosen as an example to evaluate.

Fig. 1 shows the magnetization characteristic of the evaluated SRM. The flux linkage Φ changes periodically between the aligned flux linkage Φ_a and the unaligned flux linkage Φ_u, and expressed as in (1) [9],

$$\Phi(i,\theta_m) = \Phi_u(i) + f(\theta_e)(\Phi_a(i) - \Phi_u(i)) \tag{1}$$

where $f(\theta_e)$ is the periodic function which represents the flux linkage characteristic between aligned state and unaligned state. The torque T is generated by the change of magnetic co-energy W_c depending on the saliency between the stator and rotor which is caused by the change of the rotor angle θ_m.

$$T(i,\theta_m) = \frac{\partial f(\theta_e)}{\partial \theta_m}\int_0^i (\Phi_a(i) - \Phi_u(i))di' \tag{2}$$

Note that W_c equals to the surface areas surrounded by the magnetization curve and the current axis in the magnetization characteristic.

Fig. 2 depicts the T-i-θ_m characteristic obtained by calculating the formula $T(i, \theta_m)$ at the values of the current from 20A to 250A and the rotor position. It is observed from Fig. 2 that the required current value for any torque at any rotor position can be calculated.

B. Torque sharing function (TSF)

Fig. 3 shows the example of the torque sharing function (TSF) $f_{Tx}(\theta_m)$. In this paper, the TSF $f_{Tx}(\theta_m)$ which represents the sharing rate of each phase torque according to the rotor position, is used to derive the constant-torque current waveforms. In order to make the sum of each phase's torque result in the constant torque, f_{Tx} becomes 1 during one-phase conduction period, whereas the sum of two-phase's f_{Tx} equals to 1 during two-phase conduction period (the period θ_{lap} in the figure). It is observed that various functions can be selected for the torque sharing function. In this paper, the quadratic function is utilized to avoid a steep rise. Therefore, the TSF is expressed as in (3),

$$f_{Tx}(\theta_m) = \begin{cases} \dfrac{2(\theta_m - \theta_0)^2}{\theta_{lap}{}^2} & \theta_0 \le \theta_m \le \theta_0 + 0.5\theta_{lap} \\ 1 - f_{Tx-1}(\theta_m) & \theta_0 + 0.5\theta_{lap} \le \theta_m \le \theta_{f0} \\ 1 & \theta_{f0} \le \theta_m \le \theta_{fc} \\ 1 - f_{Tx+1}(\theta_m) & \theta_{fc} \le \theta_m \le \theta_{fc} + 0.5\theta_{lap} \\ \dfrac{2(\theta_m - \theta_c)^2}{\theta_{lap}{}^2} & \theta_{fc} + 0.5\theta_{lap} \le \theta_m \le \theta_c \\ 0 & otherwise \end{cases} \tag{3}$$

where θ_{lap} represents the two-phase conduction period, and θ_{f0} indicates the initial angle of the one-phase conduction period. In the SRM with number of phases m, number of stator pole N_s, and number of rotor poles N_r structure, since the conduction period of the adjacent phase shifts the angle of $2\pi/mN_r$ rad in the mechanical angle, the turn-on angle θ_0, the ending angle θ_{fc} of the one-phase conduction period, and the turn-off angle θ_c are expressed as dependent variables of θ_{lap} and θ_{f0}. The torque of each phase is controlled accurately by the multiplication of (3) with the torque command T^*, eliminating completely the torque ripple.

In order to optimize the constant-torque current waveform, the only two dependent variables of θ_{lap} and θ_{f0} are required to

TABLE I. Motor Parameters of SRM.

	Symbol	Value
Rated mechanical power	P_m	5.5kW
Maximum speed	ω_n	12000r/min
Maximum torque	T_n	9.3Nm
Input voltage	V_{dc}	48V
Number of poles	N_s/N_r	12/18
Winding resistance	R	0.011Ω
Number of turns	N	12turns

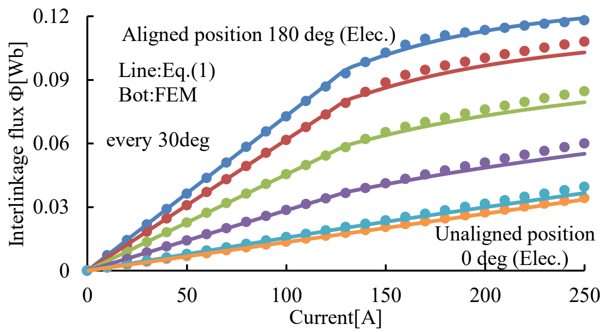

Fig. 1. Magnetization characteristic.

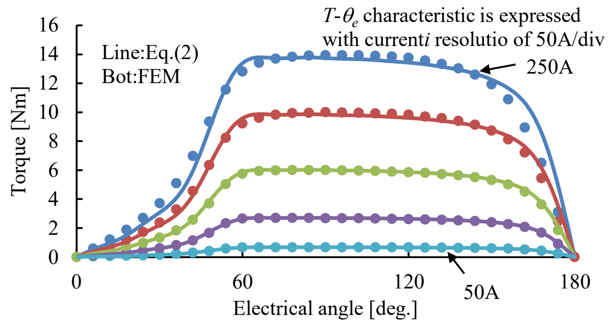

Fig. 2. T-i-θ_m characteristic.

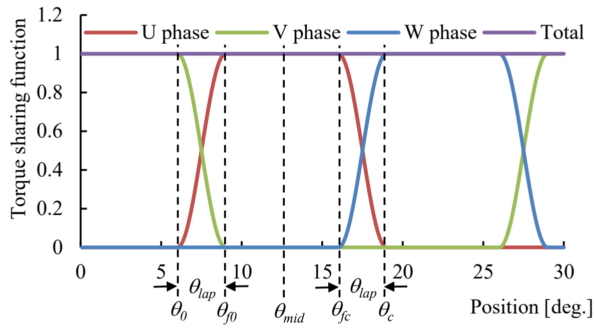

Fig. 3. Torque sharing function.

be designed in consideration of the motor current RMS value, the DC current ripple, and the radial force. In the constant-torque current waveform, θ_{lap} affects the smoothness of the current during switching phase interval, meanwhile θ_{f0} affects the excitation timing. First, the relationship between all above criteria and two variables of θ_{lap} and θ_{f0} is clarified. Next, the optimization process of θ_{lap} and θ_{f0} is explained based on the derived quantitative evaluation functions of all above criteria.

C. Motor Current RMS value minimization

The derivation method of the constant-torque current waveform with minimum motor current RMS value has been proposed in [9]. In this method, the margin M is defined as the difference between the maximum current slope, which is possible to generate by the input voltage, and the constant-torque current slope. The constant-torque current waveform is applicable when the margin M is positive. In this method, the torque per current value during the conduction period is maximized while shortening the conduction period under the condition that $M \geqq 0$ is satisfied. However, the DC current ripple increases because the current slope becomes steep. In addition, the radial force ripple also increases because the torque is obtained during the alignment state where the radial force per current value is large.

III. M ULTIPLE OBJECTICVE OPTIMIZATION

In this section, the derivation method of the constant-torque current waveform considering the motor current RMS value, the DC current ripple, and the radial force ripple reduction is explained. As explained above, in the derivation method of the constant-torque current waveform with minimized motor current RMS, the DC current ripple and the radial force ripple increase inversely with the motor current RMS value reduction. First, the relationship between all above criteria and two variables of θ_{lap} and θ_{f0} is clarified. Next, in order to optimize multiple objective functions considering a trade-off relationship, the weight function is introduced. For avoidance of time-consuming numerical process, quantitative evaluation functions of the motor current RMS value, the DC current ripple, and the radial force ripple are derived from the mathematical model. Finally, the derivation method of the desired constant-torque current waveform considering the motor current RMS value, the DC current ripple, and the radial force ripple is explained.

A. Motor current RMS value

In this subsection, the evaluation function of the motor current RMS value is derived. The motor current RMS value affects the motor efficiency. Generally, the motor current RMS value is evaluated by numerically computing the root mean square of the constant-torque current waveform in the TSF methods [5]-[8]. In this paper, the quantitative evaluation function is mathematically derived based on the characteristics of the linear region for the sake of simplicity.

Fig. 4 shows the evaluated results and simulation results of motor current RMS value. The constant-torque current waveform in linear region is expressed as in (4)[9].

$$i^*(\theta_m) = \sqrt{\frac{2T^*}{L_a - L_u}} \sqrt{f_{Tx}(\theta_m) \Big/ \frac{\partial f(\theta_e)}{\partial \theta_m}} \tag{4}$$

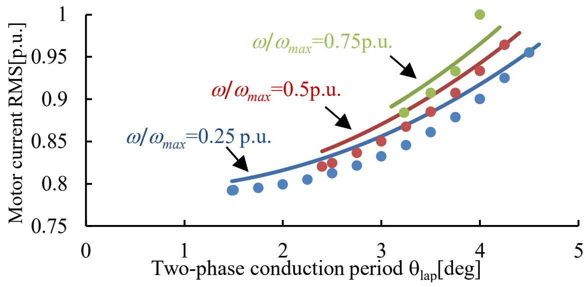

Fig. 4. Evaluated results and simulation results of Motor current RMS value.

where L_a is the initial aligned stator inductance and L_u is the unaligned stator inductance. It is mathematically impossible to formulate accurately the motor current RMS value of the constant-torque current waveform; therefore, the motor current RMS value is approximately derived as following. First, it is assumed that θ_{lap} is sufficiently shorter than one cycle. The change of the inductance during θ_{lap} is constant compared to the change of TSF. In addition, since the influence of the air gap is dominant in the inductance in one-phase period, the change of the inductance can be assumed as constant. In the approximation, the average value during each period of the inductance change is adopted, and the motor current RMS value is expressed as in (5).

$$i^*_{RMS} = \sqrt{\frac{2T^*}{L_a - L_u}} \sqrt{\frac{S_1 + S_2 + S_3}{2\pi / N_r}} \tag{5}$$

$$S_1 \approx \frac{\theta_{lap}{}^2 / 2}{f(\theta_{f0}) - f(\theta_0)} \tag{6}$$

$$S_2 \approx \frac{2\pi / mN_r - \theta_{lap}}{f(\theta_{fc}) - f(\theta_{f0})} \tag{7}$$

$$S_3 \approx \frac{\theta_{lap}{}^2 / 2}{f(\theta_c) - f(\theta_{fc})} \tag{8}$$

where S_1, S_2, and S_3 are the integral of the square of the current in the two-phase conduction period (rise), the one-phase conduction period, and the two-phase conduction period (fall), respectively. The motor current RMS value is approximated only by TSF parameters and motor parameters. In order to reduce the motor current RMS value, θ_{lap} should be short and the torque per current value during the conduction period is maximized[9].

B. DC current ripple RMS

In this subsection, the evaluation function of the DC current ripple is derived. The DC current ripple affects the lifespan of the battery. In this paper, the low frequency DC current ripple generated by the cycle of the phase current, which is related to the rotation speed of SRM, is focused. The high frequency DC current ripple generated by the switching of the converter can be reduced by applying the free-wheeling mode of the conversion [10]. In Ref. [11], the instantaneous DC current ripple is suppressed with specified current profile. However, the DC current ripple RMS cannot evaluated for not specified current profile such as the constant-torque current waveform. In this paper, the quantitative evaluation function is mathematically derived based on the characteristics in the TSF method in order to simplify the optimization process.

Fig. 5 shows the evaluated results and the simulation results of the DC current ripple RMS value. The input power P_{in} is expressed by (9).

$$P_{in} = (I_{dc} + i_{dcRip.})V_{dc} = \frac{\partial \theta_m}{\partial t}\frac{\partial W_f}{\partial \theta_m} + \frac{\partial i}{\partial t}\frac{\partial W_f}{\partial i} + T\omega \tag{9}$$

where I_{dc} is the input DC current, $i_{dcRip.}$ is the input DC current ripple, V_{dc} is the input voltage, W_f is the magnetic energy, and ω is the rotation speed. Note that W_f equals to the surface areas surrounded by the magnetization curve and the flux axis in the magnetization characteristic (cf., Fig. 1). It is assumed that the effect of the magnetic saturation is small; hence, W_c is same as W_f. As a result, the first term in the left side of (9) is considered as same as the third term which is constant value. Therefore, the input power ripple $i_{dcRip.}V_{dc}$ is calculated by the second term in the left side of (9). Since the periodic integral of the fluctuation of W_f which represents the first and second terms in the left side of (9) is zero,

$$\int_0^{\theta_{lap}} i_{dcRip.}V_{dc}\,d\theta = T\omega\frac{2\pi}{mN_r} \tag{10}$$

Since the current change is almost zero except for θ_{lap}, the integral range of the left term is θ_{lap}. It is assumed that $i_{dcRip.}$ is a linear function (triangle). According to (10), the surface of the triangle is $T\omega 2\pi/mN_rV_{dc}$ and the width is θ_{lap}. Therefore, the DC current ripple RMS is expressed as in (11).

$$i_{dcRip.RMS} = \frac{\omega T}{V_{dc}}\sqrt{\frac{2}{3}}\sqrt{\frac{2\pi/mN_r}{\theta_{lap}}} \tag{11}$$

The DC current ripple RMS values is approximated by only TSF parameters and experimental condition. In order to reduce the DC current ripple, θ_{lap} should be long which is contradictory to the motor current RMS reduction.

C. Radial force ripple

In this subsection, the evaluation function of the radial force ripple is derived. The radial force ripple affects the acoustic noise and vibration. The radial force ripple is reduced by decreasing the sum of the radial forces generated from all phases of SRM. Generally, the radial force ripple is evaluated by simulating the instantaneous radial force with radial force model and calculated its peak-to-peak [12]. However, large amount of calculation is needed. In this paper, the quantitative evaluation function is mathematically derived based on the characteristics in the TSF method in order to simplify the optimization process.

Fig. 6 shows the constant-torque current waveform and the radial forces of three phases. As shown in Fig. 6, in the constant-torque current waveform, the excitation is continued to the alignment state when the radial force per current value is large, and then the current falls. Therefore, the radial force is maximized at the ending angle of the one-phase conduction period $\theta_{fc}=\theta_{f0}-\theta_{lap}+2\pi/mN_r$ when the current starts to fall. Meanwhile, the radial force is minimized at the turn-off angle θ_c (the initial angle of the one-phase conduction period of adjacent phase) when the current is zero. Therefore, the radial force ripple is expressed as in (12),

$$F_{rSUMRip.} \approx F_r(i^*(\theta_{fc}),\theta_{fc}) - F_r(i^*(\theta_{f0}),\theta_{f0}) \tag{12}$$

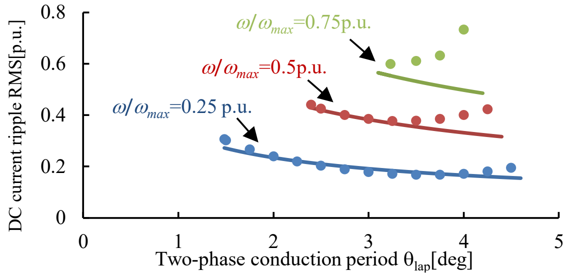

Fig. 5. Evaluated results and simulation results of DC current RMS value.

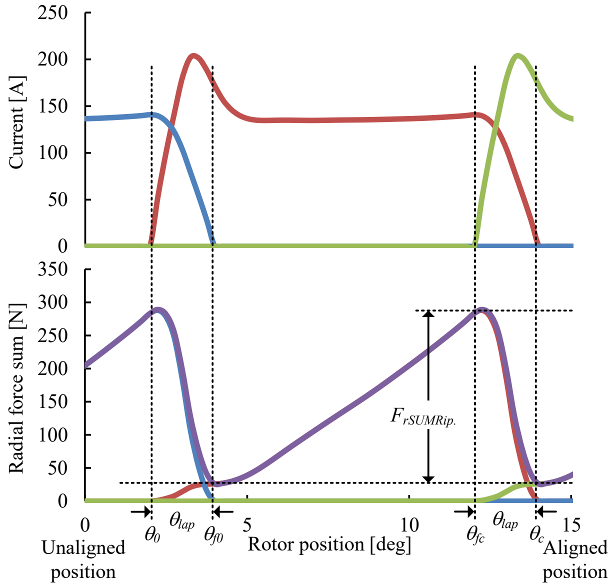

Fig. 6. Current waveform and radial force (θ_{f0}=4deg, θ_{lap}=2deg).

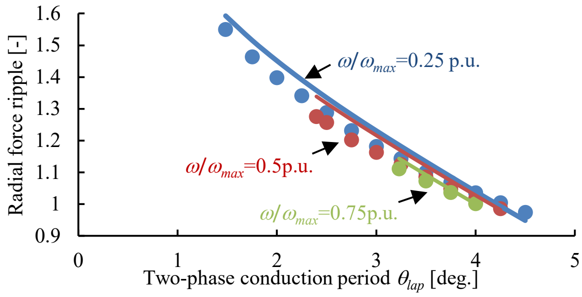

Fig. 7. Evaluated results and simulation results of radial force ripple.

where $F_r(i_m,\theta)$ of (12) is one phase radial force at the value of the current i and the rotor position θ. In order to derivate the radial force ripple, $F_r(i,\theta)$ is formulated. The radial force is expressed as in (13) from Maxwell's stress.

$$F_r(i,\theta_m) = \frac{B(i,\theta_m)^2}{2\mu_0}S_{alig}(\theta_m) = \frac{\phi_g(i,\theta_m)^2}{2\mu_0 S_{alig}(\theta_m)} \tag{13}$$

where B is the magnetic flux density, ϕ_g is the flux of air gap, μ_0 is the vacuum permeability, and S_{alig} is the surface of aligned teeth. S_{alig} is calculated from the tooth width of the rotor and stator, core thickness, and rotor position. ϕ_g is calculated from the magnetization characteristic.

Fig. 7 shows the evaluated results and simulation results of the radial force ripple. In order to reduce the radial force ripple, both the decrease in the maximum point of $\theta_{fc}=\theta_{f0}-$

θ_{lap}+2π/mN_r and the increase in the minimum point of θ_{f0} are necessary. To achieve both requirements, θ_{lap} should be long.

D. Derivation of ideal constant-torque current waveform

The motor current RMS value becomes high when the DC current ripple RMS value and radial force ripple are small, i.e. the two-phase conduction period θ_{lap} is long. Therefore, it is clear that there is a trade-off relationship between these criteria. In order to simultaneously optimize multiple objective functions considering the trade-off relationship, the weight function is introduced. The weight function g is defined as (14), (15). Note that each evaluation function is normalized by using the maximum and minimum values.

$$g = w_1 Z(i^*_{RMS}) + w_2 Z(i_{DCRip.RMS}) + w_3 Z(F_{rRip.}) \tag{14}$$

$$where \quad Z(f) = \frac{f - \min(f)}{\max(f) - \min(f)} \tag{15}$$

where $w_1+w_2+w_3=1$, and $0 \leqq w_n \leqq 1$ are satisfied. In this paper, the constant-torque current waveform is optimized considering the motor current RMS value, the DC current ripple, and the radial force ripple by using (14) and setting appropriate weight factors w_1, w_2, w_3.

Fig. 8 depicts the flowchart for the derivation of the ideal constant-torque current waveform. It is assumed that the current RMS value has been already minimized [9]. Under the consideration of the minimized current RMS value method, the DC current ripple and the radial force ripple are maximized since θ_{lap} is the shortest. In addition, the margin M_f when the current rises is positive, but the margin M_l when the current falls is derived as 0. As a result, the turn-off angle θ_c cannot be increased any further. Therefore, while fixing the turn-off angle θ_c obtained by the minimized current RMS value method, θ_{lap} is varied to minimize the weight function.

IV. MULTIPLE OBJECTICVE OPTIMIZATION

A. Simulation results

The effectiveness of the ideal constant-torque current waveform is verified by simulation. The motor parameters and the magnetization characteristic of the evaluated SRM are as shown in Table I and Fig.1. The simulation is conducted at ω/ω_{max}=0.25, T^*=4.91Nm. Note that the maximal torque-ripple-free speed (TRFS) ω_{max} is the maximum speed which can still achieve the constant torque [6].

Fig. 9 shows the constant-torque command currents, the currents, the torque, the DC current, and the radial force generated from all the phases of SRM, in two cases (a) which focuses more on the current RMS value reduction and (b) which focuses more on the radial force ripple reduction. In both cases shown in Fig. 9, an instantaneous torque without any ripple, i.e. the constant torque, is achieved. Comparing Fig. 9(a) and (b), the motor current RMS value is reduced in case of (a) which focuses more on the motor current RMS value reduction, while the radial force ripple is reduced in case of (b) which focuses more on the radial force ripple reduction. Note that the DC current ripple is also reduced even if w_3 is large. The reason is because the longer the θ_{lap} is, the smaller the DC current ripple RMS value becomes.

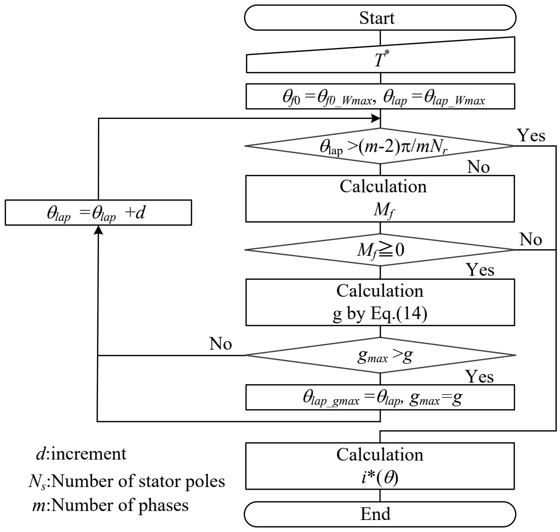

Fig. 8. Generation flow for ideal current waveform.

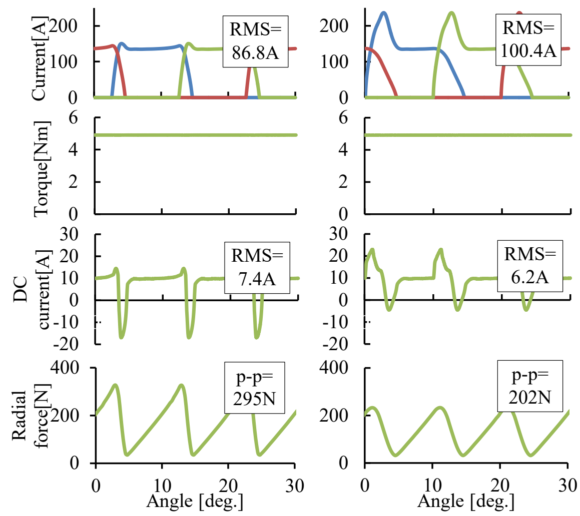

(a) w_1=0.7, w_2=0.15, w_3=0.15 (b) w_1=0.15, w_2=0.15, w_3=0.7

Fig. 9. Simulation results of the currents, the torque, the DC current, and the radial force at (T^*=4.91Nm, ω/ω_{max}=0.25).

B. Effectiveness of weight factor w

Fig. 10(a)-(c) show the relationship between the weight w and the motor current RMS value, the DC current ripple RMS value, and the radial force ripple. The horizontal axis is the weight of the corresponding value. The rotation speed is ω/ω_{max}=0.25. In Fig. 10(a)-(c), the motor current RMS value, the DC current ripple RMS value, and the radial force ripple are reduced by 18%, 45%, 37 % at most when the respective weight factors w_1, w_2, w_3 increase. Note that the DC current ripple and the radial force ripple are small even if w_3 is large as shown in Fig. 10(b) and w_2 is large in Fig. 10(c). The reason is because the longer the θ_{lap} is, the smaller the radial force ripple and the DC current ripple RMS value become. In Fig. 10(b), the DC current ripple tends to increase in the region of large weight factor, because the evaluation function of the DC current ripple is derived assuming that θ_{lap} is sufficiently short. Therefore, when θ_{lap} increases, the approximation error increases, resulting in that the tendencies do not match.

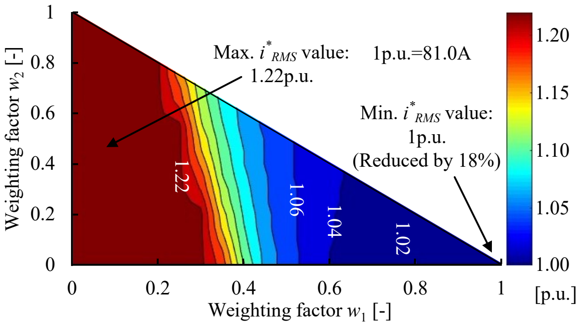

(a) Motor current RMS value

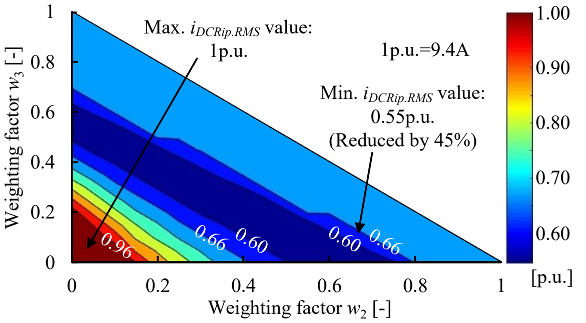

(b) DC current ripple RMS value

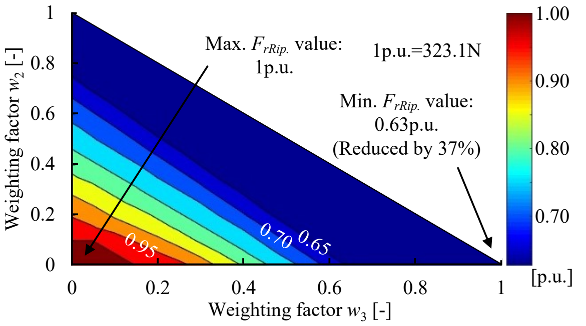

(c) Radial force ripple

Fig. 10. Relationship with weighting factors w. Note that 1 p.u. is the value when applying minimized current RMS value method. w_1: Motor current RMS value, w_2: DC current ripple RMS value, w_3: Radial force ripple.

C. Experimental results

The effectiveness of the ideal constant-torque current waveform is verified experimentally. In the experiment, the maximum hysteresis error designed to be 10A regulated by the switching of the switching devices. In order to evaluate properly the torque ripple due to the commutation, it is necessary to avoid the torsional resonance. In the test bench, the re sonant frequency is 171Hz. Therefore, the experiment is conducted at 345 r/min, 4.91Nm in which the first order frequency is 69 Hz and second order frequency is 138 Hz.

Fig. 11 and Fig.12 show the current waveforms, the torque waveforms, and the harmonic components of the torque with (a) single pulse-wise current method, the torque ripple reduction methods based on the ideal constant-torque current in two case s (b) w_1=0.7, w_2=0.15, w_3=0.15 and (c) w_1=0.15, w_2=0.15, w_3=0.7. The torque ripples of the constant-torque current waveform as shown in Fig. 11 (b) and (c) are reduced by 78.9% and 74.1 % compared with the single pulse-wise current in Fig. 11 (a), respectively. In addition, the fundamental component of the torque ripple is reduced by

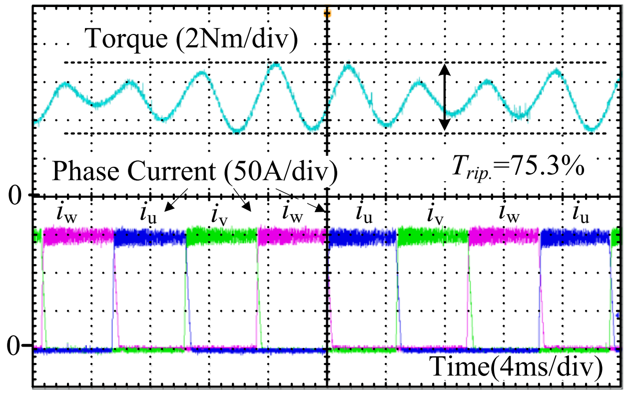

(a) Single pulse-wise current method (I_{peak}=144.7A, I_{RMS}=83.5A)

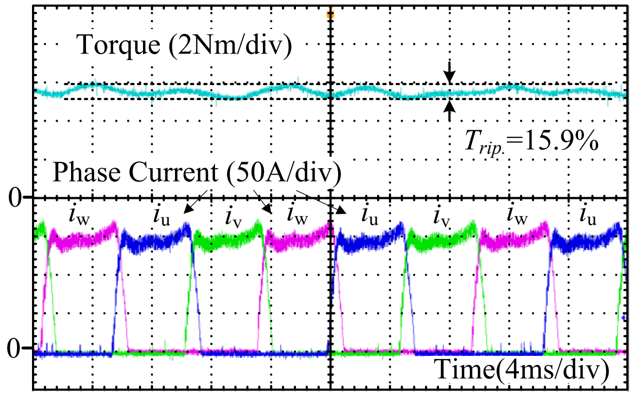

(b) w_1=0.7, w_2=0.15, w_3=0.15 (I_{peak}=160.1A, I_{RMS}=85.8A)

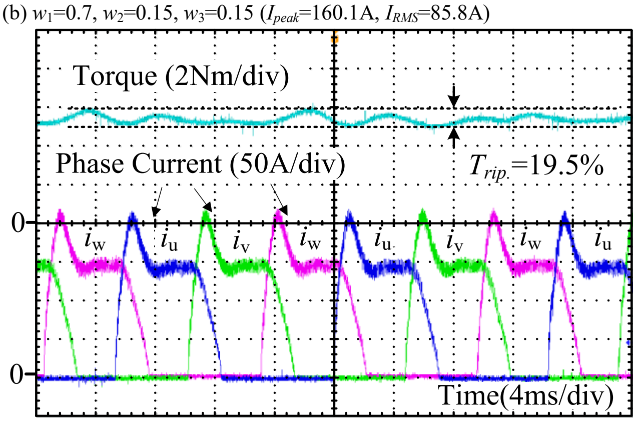

(c) w_1=0.15, w_2=0.15, w_3=0.7 (I_{peak}=209.5A, I_{RMS}=96.9A)

Fig. 11. The current waveforms, the torque waveforms at T^*=4.91Nm, Rotation speed: 345rpm.

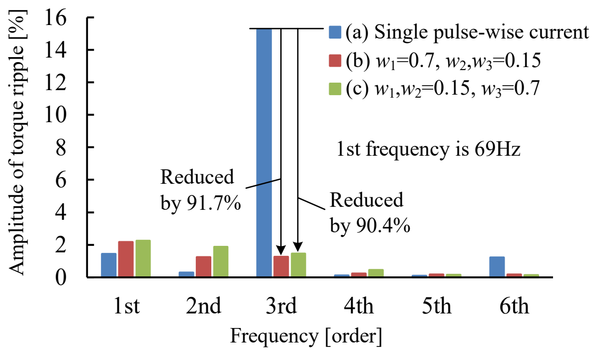

Fig. 12. The harmonic components of the torque ripple at T*=4.91Nm

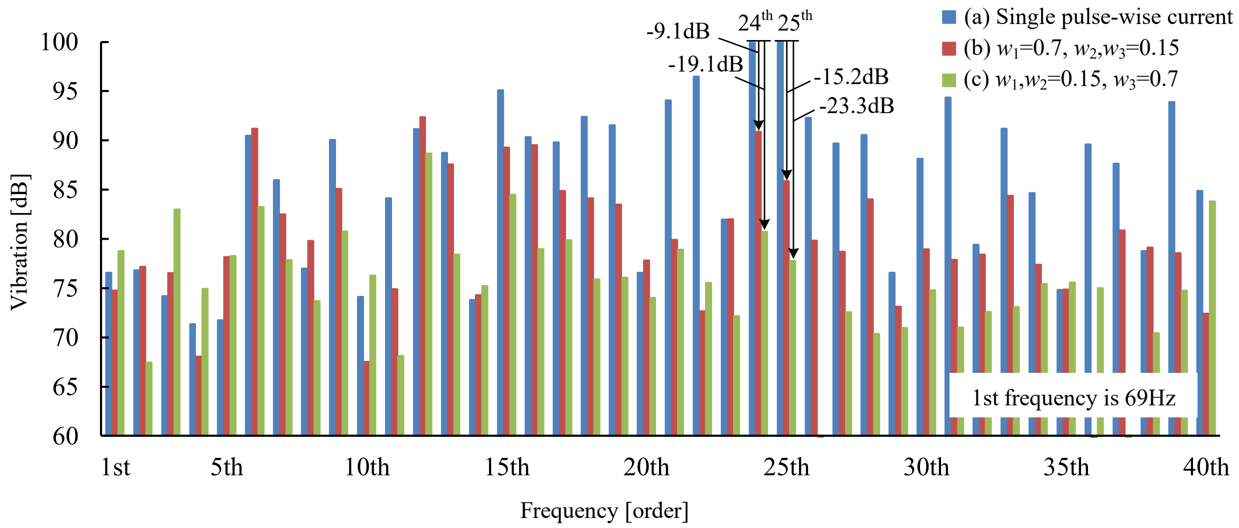

Fig. 13. The current waveforms, the torque waveforms at T^*=4.91Nm, Rotation speed: 345rpm.

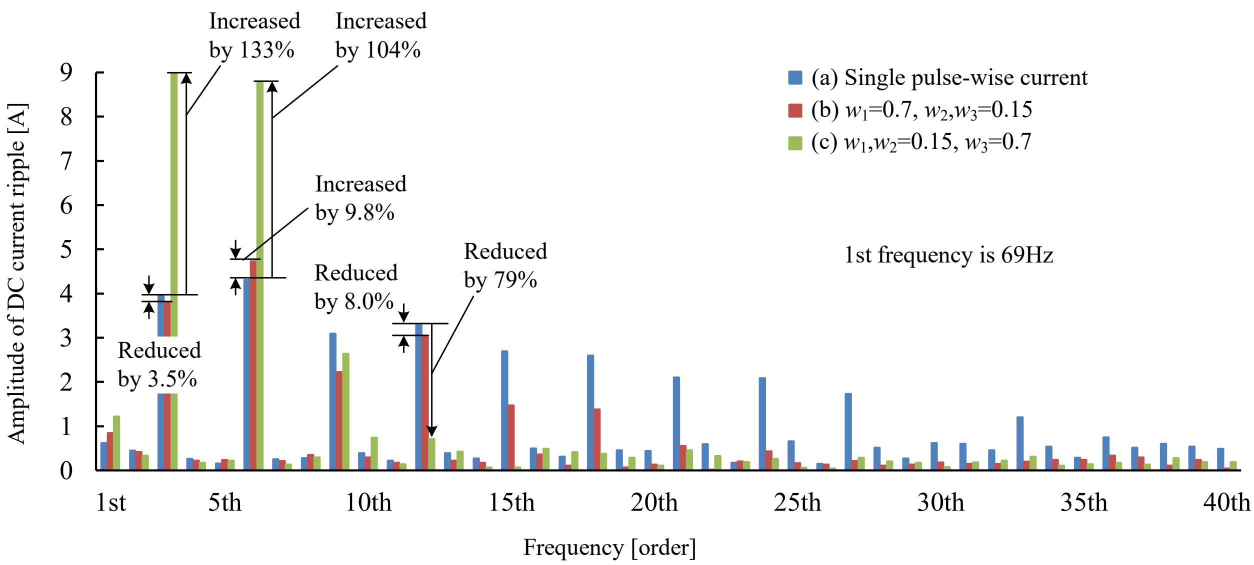

Fig. 14. The harmonic components of the DC current ripple at T^*=4.91Nm, Rotation speed: 345rpm.

91.7% and 90.4% respectively as shown in Fig. 12. In addition, comparing Fig. 9(b) and (c), the current RMS value is reduced by 11.8% in case of (b) which focuses more on the current RMS value reduction. Furthermore, the current peak value is reduced by 23.6%. Note that the torque ripple still occurs even if the constant-torque current waveform is applied. This is because the torque ripple is caused by the model inaccuracies. However, the harmonic component of the main torque ripple has already significantly reduced by around 90%.

Fig. 13 and Fig.14 show the harmonic components of the vibration and the DC current ripple generated from all the phases of SRM with (a) single pulse-wise current method, the torque ripple reduction methods based on the ideal constant-torque current in two cases (b) w_1=0.7, w_2=0.15, w_3=0.15 and (c) w_1=0.15, w_2=0.15, w_3=0.7. The 25th harmonic components which is the main vibration is reduced by 23.3 dB and 8.1 dB in case of (c) which focuses more on the radial force ripple reduction compared with (a) the single pulse-wise current and the case of (b) which focuses more on the current RMS value reduction. On the other hand, as shown in Fig. (14), the DC current ripple RMS value is not reduced in the experiment. Especially, the low frequency components of the DC current ripple are increased, although the high frequency component of the DC current ripple are reduced. As shown in Fig. 9 (b), the time width of the DC current ripple is increased, although the peak of the DC current ripple is decreased. As a result, low frequency components of DC current ripple increases instead of reducing the high frequency components.

V. Conclusion

This paper proposed the current RMS value, the DC current ripple, and the radial force ripple reduction method under zero torque ripple for SRM. In order to optimize multiple objective functions considering the trade-off relationship, the weight function was introduced. In particular, quantitative evaluation functions of the motor current RMS value, the DC current ripple, and the radial force ripple are derived from the mathematical model for avoidance of time-consuming numerical process**.** The reduction of the current RMS value, the DC current ripple, and the radial force ripple by 18%, 45%, and 37%, respectively, were achieved respectively by the proposed method.

In the future work, the accuracy of the objective functions will be improved. In addition, the experimental results will be obtained in order to validate the effective of the DC current ripple reduction.

REFERENCES

[1] I. Husain, M. Ehsani: "Torque Ripple Minimization in Switched Reluctance Motor Drives by PWM Current Control", IEEE Trans., vol.11, no.1 (1996)

[2] K. Russa, I. Husain, M. Elbuluk, "Torque-Ripple minimization of switched reluctance machines over a wide speed range", IEEE Trans. On Industry Applications, vol. 34, no. 5, pp. 1105-1112, 1998.

[3] P.C. Kjaer, J.J. Gribble, and T.J.E. Miller, "High-grade control of switched reluctance machines,"*IEEE Trans. Industrial Application*, vol. 33, no. 6, pp. 1585-1593, Nov/Dec. 1997.

[4] H. ISHIKAWA, Y. KAWADA, and H NAITOH, "Instantaneous Current Profile Control for Flat torque of Switched Reluctance Motors", Electrical Engineering in Japan, Vol. 163, No.3, 2008.

[5] Vladan P. Vujičić, "Minimization of Torque Ripple and Copper Losses in Switched Reluctance Drive," IEEE Trans. Power Electron., vol. 27, no. 1, pp. 388-399, Jan. 2012.

[6] X. D. Xue, K. W. E. Cheng, and S. L. Ho, "Optimization and Evaluation of Torque-Sharing Functions for Torque Ripple Minimization in Switched Reluctance Motor Drives," IEEE Trans. Power Electron., vol. 24, no. 9, pp. 2076-2090, Sep. 2009.

[7] Haoding Li, Berker Bilgin, and Ali Emadi, "An Improved Torque Sharing Function for Torque Ripple Reduction in Switched Reluctance Machines," IEEE Trans. Power Electronics., vol. 34, no. 2, pp. 1635-1644, Feb. 2019.

[8] Jin Ye, Berker Bilgin, and Ali Emadi, "An Offline Torque Sharing Function for Torque Ripple Reduction in Switched Reluctance Motor Drives," IEEE Trans. Energy Conversion., vol. 30, no. 2, pp. 726-735, Jun. 2015.

[9] T. Kumagai and J. Itoh, "Torque Ripple Reduction Method with Minimized Current RMS Value for SRM Based on Mathematical Model of Magnetization Characteristic", EPE2018, Vol. LS2d, No. 368 (2018).

[10] R. Krishnan: "SWITCHED RELUCTANCE MOTOR DRIVES Modeling, Simulation, Analysis, Design, and Application", CRC Press LLC (2001)

[11] T. Kusumi, T. Hara, K. Umetani, and E. Hiraki, "Simple control technique to eliminate source current ripple and torque ripple of switched reluctance motors for electric vehicle propulsion", IECON 2016, pp. 1876-1881(2016).

[12] J. Furqani, M. Kawa, K. Kiyota, and A. Chiba: "Current Waveform for Noise Reduction of a Switched Reluctance Motor under Magnetically Saturated Condition", IEEE Trans. Industrial Application, Vol.54, No.1 pp.213-222 (2018)